Int. J. Electrochem. Sci., 13 **(2018)** 2010 – 2021, doi: 10.20964/2018.02.62

International Journal of
ELECTROCHEMICAL
SCIENCE
www.electrochemsci.org

Titanium-doped P2-type $Na_{0.67}Co_{0.67}Mn_{0.33-\chi}Ti_{\chi}O_2$ ($0 \leq \chi \leq 0.2$) as Novel Cathodes for Sodium Ion Batteries with Superior-Rate

Dengmei Zhou[1], *Wanxia Huang*[1,*], *Xueya Kang*[1], *Fenglin Zhao*[1], *Ling Zhao*[1], *Zhilin Deng*[2], *Xianwei Yan*[2], *Yongbo Yu*[2], *Mingwu Xiang*[1]

[1] College of Materials Science and Engineering, Sichuan University, Chengdu 610065, China
[2] Sichuan Guorun New Materials Co.,Ltd, Meishan 620010, China
[*]E-mail: huangwanxia@scu.edu.cn

Received: 9 October 2017 / *Accepted:* 8 December 2017 / *Published:* 28 December 2017

Sodium ion batteries (SIBs) have attracted increasing attention due to the naturally abundant and inexpensive sodium resources. The layered transition metal oxides are proposed for advanced cathode materials of SIBs. However, the phase transformation and rate performance of layered compounds are still a pivotal challenges. Here，we report a series of Ti-doped $Na_{0.67}Co_{0.67}Mn_{0.33-\chi}Ti_{\chi}O_2$ ($0 \leq \chi \leq 0.2$) samples as cathodes for SIBs. As a result, the multiphase transition during the charge-discharge was successfully prohibited by partial Ti doped. It is found that the $Na_{0.67}Co_{0.67}Mn_{0.23}Ti_{0.1}O_2$ cathode exhibited superior rate performance and tremendous capacity retention. Particularly, the $Na_{0.67}Co_{0.67}Mn_{0.23}Ti_{0.1}O_2$ cathode delivers a initial discharge capacity of about 91.2 mAh g^{-1} at 1C. More attractively, even at high current rates (10, 15, 20 and 30 C), superior rate capability is achieved while retaining tremendous capacity retention. Nearly 81.02% of the initial capacity was retained after 1000 charge/discharge cycles at 20 C (3.42A g^{-1}). Therefore, Ti-doped $Na_{0.67}Co_{0.67}Mn_{0.23}Ti_{0.1}O_2$ may be a promising cathode material for SIBs with excellent rate and cycling performance.

Keywords: Sodium ion batteries; Cathode materials; $Na_{0.67}Co_{0.67}Mn_{0.33-\chi}Ti_{\chi}O_2$; Titanium-doping; High-rate

1. INTRODUCTION

As the extensive application of lithium ion batteries (LIBs) in hybrid electrical vehicles (HEVs), and electrical vehicles (EV), the demand of metal lithium grows rapidly around the world [1-3]. However，the availability and rising cost of metal lithium have driven researchers to explore rational sustainable energy-storage alternatives [4]. Owing to the abundant storage of sodium in the earth's crust and its environmentally benign，sodium-based rechargeable batteries have drawn

considerable attentions in the energy-storage system [5-8]. Recently, various cathode materials including layered transition metal oxides, phosphates, and fluorophosphates have been investigated for sodium ion batteries (SIBs) [9-13]. Among these cathode materials, the layered transition metal oxides $NaMO_2$ (M=Ni, Co, Fe, Mn and Mg elements) with unique structure and enhanced electrochemical performance have received great interest [14]. On the basis of the coordination of the Na cations and the number of transition metal layers in the repeated stacking unit, the layer $NaMO_2$ oxides are mainly categorized into P2, P3, and O3 types [15].

Na_XCoO_2 have been considered to be promising cathode material of SIBs because of its relatively high energy density (~260 $Wh\cdot kg^{-1}$) , fast Na^+ diffusion arising from the similar layered structure of $LiCoO_2$ [16]. There exists three structure types in the hexagonal Na_XCoO_2, which has been demonstrated by neutron powder diffraction [17]. Nevertheless, the P2-phase $Na_{0.74}CoO_2$ easily cause a series of phase transitions including single-phase or two phase transition during charge-discharge [18,19]. In generally, the pristine $Na_\chi CoO_2$ without any modification reported in the literatures exhibits poor electrochemical performance [18,20]. The different doping strategies, including binary/ternary transition metal cations, have been widely adopted to address the forementioned issues. Carlier et al. reported that the P2-$Na_{2/3}Co_{2/3}Mn_{1/3}O_2$ exhibited a stable layer structure due to the coexistence of Co^{3+} and Mn^{4+} [21]. Correspondingly, different composition of Co-based $Na_{0.66}Co_{0.5}Mn_{0.5}O_2$ [22], $NaCo_{1/2}Fe_{1/2}O_2$[23], $Na_\chi Co_{0.7}Mn_{0.3}O_2$ ($\chi\approx1$) [9], $Na_{0.7}Co_{1-y}Mn_yO_2$ [24] have been reported as cathode materials of SIBs. Shen et al. reported manganese-doped P2-$Na_\chi Co_{0.7}Mn_{0.3}O_2$, which showed attractive reversible capacity (95 mAh g^{-1} between 2.0 and 4.1V at 1C) and excellent cycling performance (84% capacity retention after 225 cycles at 1C rate) [9]. In addition, the cation co-doped ternary systems such as $NaNi_{1/3}Mn_{1/3}Co_{1/3}O_2$ [25], $NaNi_{1/3}Co_{1/3}Fe_{1/3}O_2$ [26], $Na_{2/3}Co_{2/3}Mn_{2/9}Ni_{1/9}O_2$ [27], $NaMn_{0.33}Ni_{0.33}Co_{0.33}O_2$ [28] also emerge successively, which significantly stabilize structure in the cathode materials and improve the capacity retention of SIBs. For instance, the $Na_{2/3}Co_{2/3}Mn_{2/9}Ni_{1/9}O_2$ reported by Doubaji et al. delivers a high discharge capacity of 110 mAh g^{-1} with a capacity retention of 89% after 90 cycles at C/20. Although great progresses in the previous reports, the conspicuous existence of multiphase transitions during Na^+ intercalation/deintercalation process lead to the degenerative capacity and poor rate capability in SIBs. To address this issue, doping a small amount of electrochemically inactive element into the transition metal oxide layer is proved to be viable approach in inhibiting the phase transition, such as Ti and Mg has been widely adopted in Ni-based and Mn-based sodium ion batteries [29-32]. Considering the similar ionic radii and same valence between Mn^{4+} (53 pm) and Ti^{4+} (60.5 pm), Sun et al. synthesized a series of $NaNi_{0.5}Mn_{0.5-X}Ti_XO_2$, which indicates that partial Ti substitution could suppress the irreversible multiphase transformation and retain a better cycle retention and higher rate performance [30]. Besides, the stepwise profiles of $Na_{2/3}Ni_{1/3}Mn_{2/3}O_2$ obviously changed upon titanium substitution reported by Komaba et al., suggesting the suppression of phase transition during sodium intercalation [29]. As far as we know, relatively less research is focused on the field of Co-based layered transition metal oxide. Herein, improving the electrochemical performance and simultaneously suppressing the multiphase transitions are a vital challenge in the future.

In this study, various of Ti-doped P2-$Na_{0.67}Co_{0.67}Mn_{0.33-\chi}Ti_\chi O_2$ cathode materials were successfully synthesized by a facile solid-state reaction. The effects of titanium-doping amount in the x

range of 0 to 0.2 on the structure and electrochemical performance were investigated in detail. Consequently, the substitution of Co with Ti in P2-$Na_{2/3}Co_{2/3}Mn_{1/3}O_2$ demonstrates that the Ti-doping stabilize a good P2-type structure and significantly suppress the phase transition during the charge-discharge. On the basis of the unique merits, the $Na_{0.67}Co_{0.67}Mn_{0.23}Ti_{0.1}O_2$ cathode shows excellent rate capacity and cycling stability with a high reversible capacity of 86.75 mAh g^{-1} after 120 cycles at a current rate of 1C. This work indicates that the $Na_{0.67}Co_{0.67}Mn_{0.23}Ti_{0.1}O_2$ cathode may be a potential candidate towards the future development of SIBs.

2. EXPERIMENTAL

2.1. Materials preparation

The $Na_{0.67}Co_{0.67}Mn_{0.33-\chi}Ti_{\chi}O_2$ (χ=0.0, 0.05, 0.1, 0.15 and 0.2) samples were synthesized by a conventional one step solid state reaction method. Na_2CO_3, Co_3O_4, Mn_3O_4 and TiO_2 powders were used as raw material with the stoichiometric ratio and homogenously mixed by wet ball-milling in ethanol solution, then dried at 80^{o}C for 12h. An excess of 5 mol% Na_2CO_3 was used to compensate for Na_2O evaporation on firing. The dried powders were calcined at 900°C in oxygen to obtain the desired electrode materials.

2.2. Materials characterization

The crystal structure of as-prepared materials was determined by X-ray diffraction (XRD, Rigaku D/max 2500 PC) in the 2θ range of 10°-80°. The morphologies were studied by scanning electron microscopy (SEM, Hitachi S-4800). Elemental composition analysis was performed by inductively coupled plasma-atomic emission spectroscopy (ICP-AES, PE Optima-8000).

2.3. Electrochemical measurement

2032-type Coin cells were assembled using metallic sodium as the anode electrode, and the composite cathode was obtained by active material (80wt%), acetylene black (10wt%), and polyvinylidene fluoride (PVDF, 10wt%) in appropriate amount of N-methyl-2-pyrrolidene (NMP) coated on aluminum foil current collectors. 1M $NaClO_4$ dissolved in a mixture of 1:1:1 ethylene carbonate (EC)/dimethyl carbonate (DMC)/ethyl methyl carbonate (EMC) (1:1:1 in volume) with 5 vol% FEC was used as the electrolyte, and the glass fiber GF/D (Whatman) was used as the separator. All the cells were assembled in Ar-filled gas glove box. Galvanostatic charge-discharge tests were performed using a NEWARE BTS-5V10 mA battery tester between 2 V and 4.2 V under various rates. Cyclic voltammetry (CV) and electrochemical impedance spectroscopy (EIS) tests were conducted on a CHI660C electrochemical workstation. The CV tests were carried out over the potential range of 2.0 V and 4.2 V at a scanning rate of 0.1-1 mV/s. The EIS spectra were taken in a range of 100 KHz to 0.01 Hz with an input signal amplitude of 5 mV.

3. RESULTS AND DISCUSSION

3.1. Structure and morphology

Fig.1a shows the XRD patterns of the as-prepared $Na_{0.67}Co_{0.67}Mn_{0.33-\chi}Ti_{\chi}O_2$ with different Ti-doping amounts.

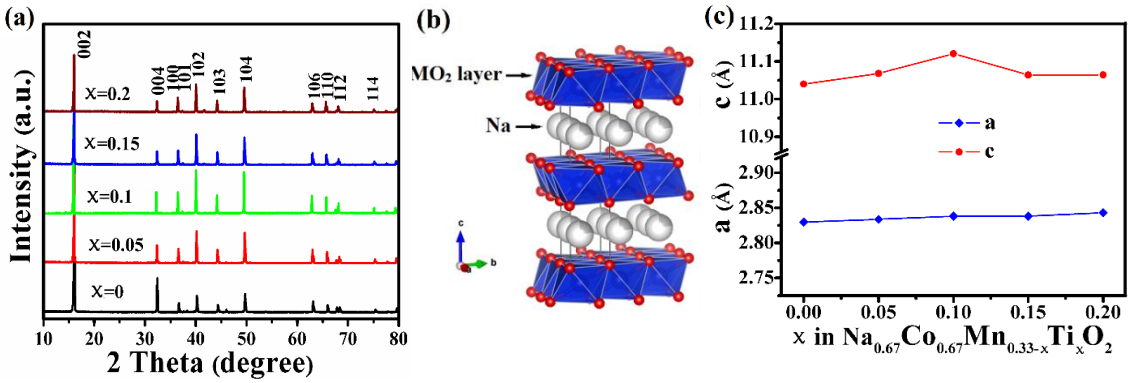

Figure 1. (a) XRD patterns of the $Na_{0.67}Co_{0.67}Mn_{0.33-\chi}Ti_{\chi}O_2$ with different Ti-doping amounts, (b) schematic illustration of the P2-type layered transition metal oxides, and (c) the corresponding lattice parameters.

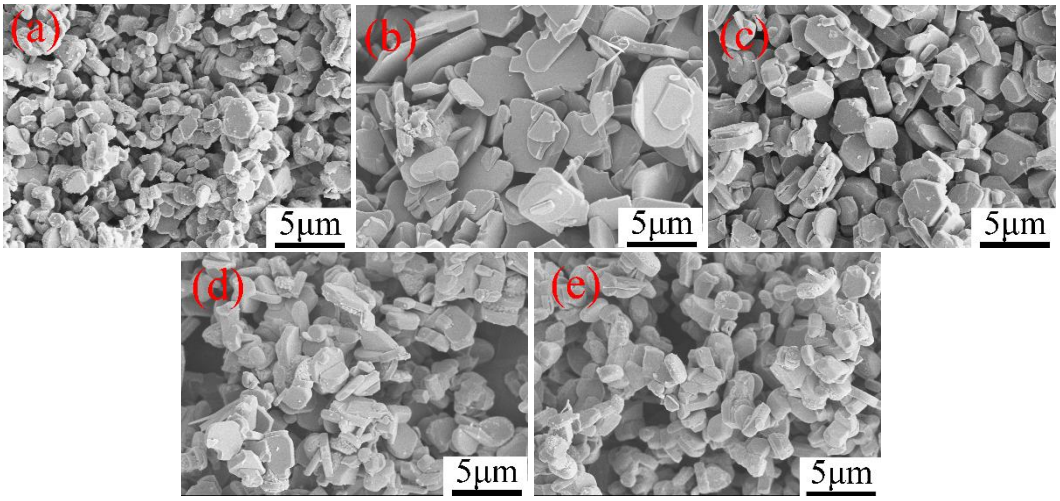

Figure 2. SEM images of the $Na_{0.67}Co_{0.67}Mn_{0.33-\chi}Ti_{\chi}O_2$, (a) χ=0, (b) χ=0.05, (c) χ=0.1, (d) χ=0.15, and (e) χ=0.2.

As shown, all the XRD patterns exhibit similar characteristic diffraction peaks which corresponds to the P2-structure with space group P63/mmc [33,34]，where Titanium ions are located in the transition metal oxide layer [35,32]. Moreover, the sharp peaks of these samples indicate good crystal structure. Especially, with the elevated Ti content，the intensity of (102) and (104) crystal planes gradually increase up to a maximum value atχ=0.1, and then decrease. In addition, the (004)

plane shows a reduced trend. A schematic illustration of the P2-type layered transition metal oxides is also shown in Fig.1b. The derived lattice parameters are summarized in Fig.1c. Lattice parameters in the a-axis linearly increase with elevated Ti content, while the c-axis is maximized at χ=0.1. These results suggest that a solid solution is formed in the range of $0 \leq \chi \leq 0.2$ in $Na_{0.67}Co_{0.67}Mn_{0.33-\chi}Ti_{\chi}O_2$ [29,36].

The morphological features and particle size of the $Na_{0.67}Co_{0.67}Mn_{0.33-\chi}Ti_{\chi}O_2$ with various Ti content were depicted in Fig. 2a-e respectively. SEM images show analogous hexagonal plate-like particles. The pristine andχ=0.05 sample exhibts irregular particles with the size between 0.5 and 5μm. With the increased Ti-doping, the sample χ=0.1, 0.15 and 0.2 showed homogeneous particles with a diameter of 1-3μm. Especially a uniform size distribution is achieved in the $Na_{0.67}Co_{0.67}Mn_{0.23}Ti_{0.1}O_2$.

3.2. Elemental analysis

ICP-OES technique was performed to determine the chemical composition of all the as-prepared $Na_{0.67}Co_{0.67}Mn_{0.33-X}Ti_XO_2$ materials, and the results are presented in Table 1. Experimentally, these test results are in good agreement with the theoretical values of the designed $Na_{0.67}Co_{0.67}Mn_{0.33-\chi}Ti_{\chi}O_2$ (χ=0, χ=0.05, χ=0.1, χ=0.15, χ=0.2).

Table 1. ICP-AES result of typical P2-type $Na_{0.67}Co_{0.67}Mn_{0.33-\chi}Ti_{\chi}O_2$ (χ=0, χ=0.05, χ=0.1, χ=0.15, and χ=0.2) samples.

Theoretical chemical formula	**Measured atomic ratio**				**Na/M**
	Na	**Co**	**Mn**	**Ti**	
$Na_{0.67}Co_{0.67}Mn_{0.33}O_2$	0.668	0.654	0.319	0	**0.686**
$Na_{0.67}Co_{0.67}Mn_{0.28}Ti_{0.05}O_2$	0.673	0.649	0.291	0.055	**0.674**
$Na_{0.67}Co_{0.67}Mn_{0.23}Ti_{0.1}O_2$	0.669	0.656	0.222	0.111	**0.675**
$Na_{0.67}Co_{0.67}Mn_{0.18}Ti_{0.15}O_2$	0.681	0.648	0.188	0.166	**0.678**
$Na_{0.67}Co_{0.67}Mn_{0.13}Ti_{0.2}O_2$	0.7	0.648	0.137	0.223	**0.692**

3.3. Electrochemical properties

Fig. 3a compares the initial charge-discharge curves of the $Na_{0.67}Co_{0.67}Mn_{0.33-\chi}Ti_{\chi}O_2$ cathodes (χ=0, 0.05, 0.1, 0.15, and 0.2) tested between 2.0 V and 4.2 V at 1 C (1 C=171 mAh g^{-1}). All the cathodes show typical charge-discharge profiles of SIBs, indicating a good electrochemical reaction. The initial discharge capacities of the $Na_{0.67}Co_{0.67}Mn_{0.33-\chi}Ti_{\chi}O_2$ cathodes are 83.6, 85.1, 91.0, 84.6, and 81.5 mAh g^{-1} for χ=0, 0.05, 0.1, 0.15, and 0.2, respectively. For the $Na_{0.67}Co_{0.67}Mn_{0.33}O_2$ cathode without Ti-doping, several voltage steps are clearly observed during the charge-discharge, suggesting severe multiphase transition. Apparently, with the increased content of the Ti-doping, the voltage steps decrease and then disappear atχ=0.1, 0.15, and 0.2, indicating that the partial substitution of manganese

with titanium may suppress Na/vacancy ordering or phase transition during sodium intercalation [29,37,38]. Therefore, the $Na_{0.67}Co_{0.67}Mn_{0.23}Ti_{0.1}O_2$ with optimized Ti-doping display the highest discharge capacity.

The corresponding cycling performance of $Na_{0.67}Co_{0.67}Mn_{0.33-\chi}Ti_{\chi}O_2$ cathodes was shown in Fig. 3b. All the electrodes exhibit remarkable cycling stability up to 120 cycles at 1 C. Note that the electrode $Na_{0.67}Co_{0.67}Mn_{0.23}Ti_{0.1}O_2$ delivers the highest discharge capacity compared to the other samples during the 120 cycles. The sample χ= 0.15 and 0.2 show higher capacity retention with 96.2% and 97.0% compared than other samples χ=0 (93.5%), χ=0.05 (94.3%) and χ=0.1 (95.3%) after 120 cycles, respectively. As forementioned results, the $Na_{0.67}Co_{0.67}Mn_{0.23}Ti_{0.1}O_2$ delivers the optimal electrochemical performance. Fig. 3c and d present the charge-discharge curves of $Na_{0.67}Co_{0.67}Mn_{0.33}O_2$ and $Na_{0.67}Co_{0.67}Mn_{0.23}Ti_{0.1}O_2$ at different cycles. The charge/discharge capacity of $Na_{0.67}Co_{0.67}Mn_{0.33}O_2$ without Ti doping in the 1^{st} , 25^{th},50^{th}, 100^{th}, 120^{th} cycles are only 84.1/83.8, 83.3/82.7, 82.5/81.9, 80.2/79.5, and 79.1/78.3 mAh g^{-1} , respectively. What's more, for $Na_{0.67}Co_{0.67}Mn_{0.33}O_2$, the voltage profiles exhibit three plateaus and steps located at about 3.5, 3.7 and 4.0 V, which reflects various phase transformations [30,39]. However, the $Na_{0.67}Co_{0.67}Mn_{0.23}Ti_{0.1}O_2$ shows smooth charge-discharge profiles without voltage steps and delivers high charge/discharge capacity of 91.2/91.2, 91.3/90.5, 90.4/89.9, 88.9/88.0, and 87.4/86.7 mAh g^{-1} in the 1^{st}, 25^{th}, 50^{th}, 100^{th}, 120^{th} cycles, respectively. It maybe contribute to the suppression of phase transformation by Ti substitution upon charge-discharge and thus stabilize the structure of the electrode [40,29].

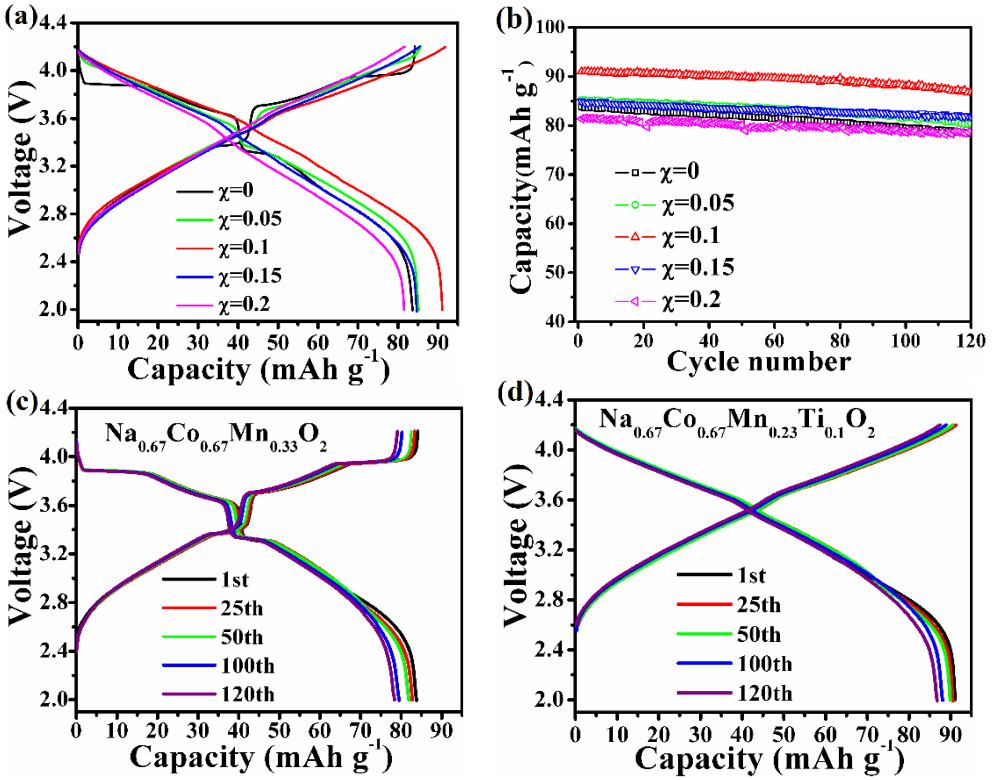

Figure 3. (a) Initial charge-discharge profiles and (b) cycling performance of the $Na_{0.67}Co_{0.67}Mn_{0.33-\chi}Ti_{\chi}O_2$ (χ=0, 0.05, 0.1, 0.15, 0.2) cathodes at 1C. Charge-discharge curves of (c) $Na_{0.67}Co_{0.67}Mn_{0.33}O_2$ and (d) $Na_{0.67}Co_{0.67}Mn_{0.23}Ti_{0.1}O_2$ at different cycles.

To further compare the electrochemical properties of the as-prepared $Na_{0.67}Co_{0.67}Mn_{0.33}O_2$ and $Na_{0.67}Co_{0.67}Mn_{0.23}Ti_{0.1}O_2$ samples, the rate capability tests were also carried out between 2.0 V and 4.2 V from 0.2 to 5C. As shown in Fig. 4a, the $Na_{0.67}Co_{0.67}Mn_{0.23}Ti_{0.1}O_2$ sample shows a better rate capacity than that of $Na_{0.67}Co_{0.67}Mn_{0.33}O_2$, which is due to the Ti-soping suppress the stepwise, also improves the rate performance. Therefore, the $Na_{0.67}Co_{0.67}Mn_{0.23}Ti_{0.1}O_2$ delivers high discharge capacities of 86.9, 90.4, 91.1, 91.4 and 91.1 mAh g^{-1} at the various rate of 0.2 C, 0.5 C, 1 C, 2 C and 5 C, respectively，Compared to the relatively low discharge capacity of 84.7, 84.6, 84.1 ，84.2 and 84.2 mAh g^{-1} for the $Na_{0.67}Co_{0.67}Mn_{0.33}O_2$ cathode. In addition, the almost complete recovery of the initial value of 1C after cycling at the high rate of 5C, gives a further proof of the structure stability [41,42]. The result figure gives a clear evidence of fast insertion/extraction of Na^+ during the charge and discharge. The voltage profiles of $Na_{0.67}Co_{0.67}Mn_{0.33}O_2$ and $Na_{0.67}Co_{0.67}Mn_{0.23}Ti_{0.1}O_2$ at different current rates ranging from 0.1 to 5C are presented in Fig. 4b and c. The profiles of $Na_{0.67}Co_{0.67}Mn_{0.33}O_2$ involve several voltage plateaus and steps at different current rates, compared to the smoothing charge-discharge profiles of $Na_{0.67}Co_{0.67}Mn_{0.23}Ti_{0.1}O_2$, which indicate that the multiphase transition was prohibited by Ti-doping.

Fig. 4d compared the Cyclic Voltammogram (CV) plots of $Na_{0.67}Co_{0.67}Mn_{0.33}O_2$ and $Na_{0.67}Co_{0.67}Mn_{0.23}Ti_{0.1}O_2$ in the voltage range of 2.0-4.2 V at a scan rate of 0.1 mV s^{-1}. Three redox peaks are observed at about 3.38/3.33, 3.73/3.66, and 3.98/3.87 V respectively for $Na_{0.67}Co_{0.67}Mn_{0.33}O_2$, which corresponds to the multiphase change [43-45]. This result is well in accordance with the charge-discharge profiles (Fig. 4b). Note that the $Na_{0.67}Co_{0.67}Mn_{0.23}Ti_{0.1}O_2$ displays only two pairs of redox couple due to the presence of Co and Mn, conforming the phase transition is effectively restrained by Ti-doping to some extent. These results could be as a good explanation of the enhanced electrochemical performance for the $Na_{0.67}Co_{0.67}Mn_{0.23}Ti_{0.1}O_2$. Nevertheless, the interrelation between the change of the crystal structure and the phase transitions during the charge and discharge need to be further investigated [46,47].

To validate the superior rate capability of $Na_{0.67}Co_{0.67}Mn_{0.23}Ti_{0.1}O_2$, the as-prepared cells were tested at higher current rates of 10, 15, 20 and 30 C, as shown in Fig.5. Clearly, the cells showed exceptional stability with high capacity retention after 1000 charge/discharge cycles. The discharge capacity of 83.9 mAh g^{-1} was obtained at 10C, which can remained 69.1 mAh g^{-1} at the higher rate of 30 C. When cycled at 20C, the cell still displayed remarkable steady, 81.02% of the initial discharge capacity remained after 1000 cycles. As a result， it can be demonstrated that P2-type $Na_{0.67}Co_{0.67}Mn_{0.23}Ti_{0.1}O_2$ equipped with superior rate remarkable cycling stability. The performance of the aforementioned materials and $Na_{0.67}Co_{0.67}Mn_{0.23}Ti_{0.1}O_2$ are partially summarized in table 2.

To further investigate the effect of scan rate on the shape and peak current of CV, the CV plots of $Na_{0.67}Co_{0.67}Mn_{0.33}O_2$ and $Na_{0.67}Co_{0.67}Mn_{0.23}Ti_{0.1}O_2$ at different scan rates ranged from 0.1 to 1mV s^{-1} are shown in Fig. 6a and b. The anodic peaks shift to a more positive potential, while the cathodic current in sequence shift to a more negative potential position with the increase of scan rates. The redox peak separation increases in sequence with the increasing of scan rate, indicating in greater loss of capacity, which is most probably due to the polarization of the electrode [48].

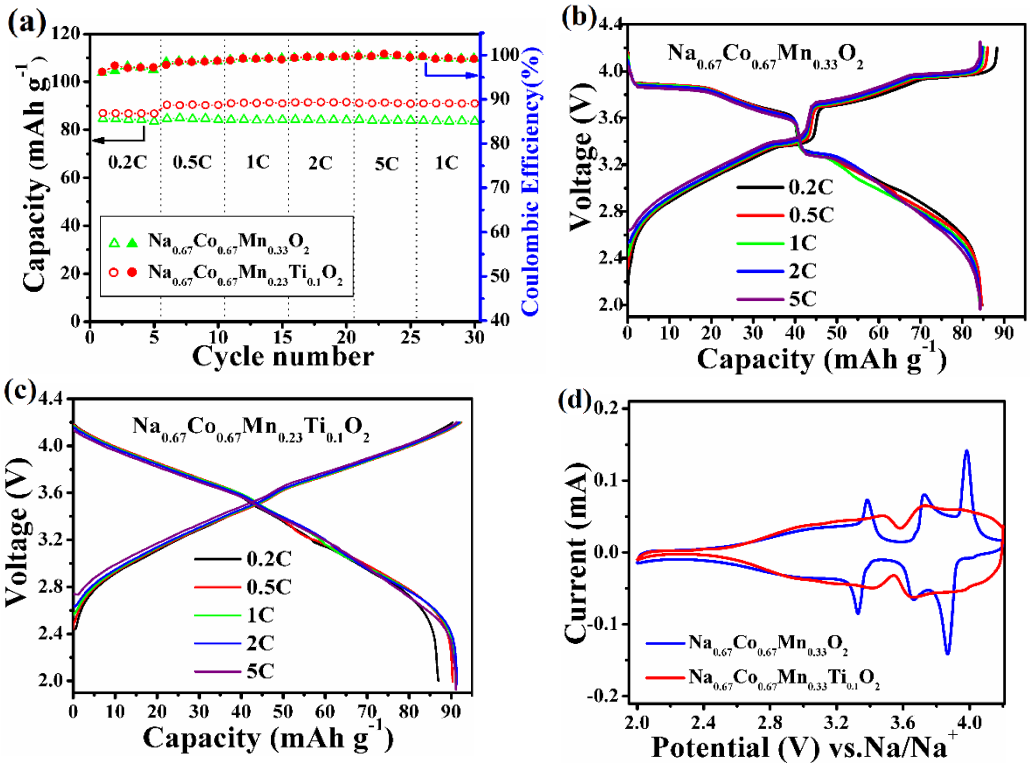

Figure 4. Electrochemical performance comparison of $Na_{0.67}Co_{0.67}Mn_{0.33}O_2$ and $Na_{0.67}Co_{0.67}Mn_{0.23}Ti_{0.1}O_2$ samples: (a) rate performance and coulombic efficiency, (b-c) charge-discharge curves at different C rates, (d) CV curves at a scan rate of 0.1 mV/s.

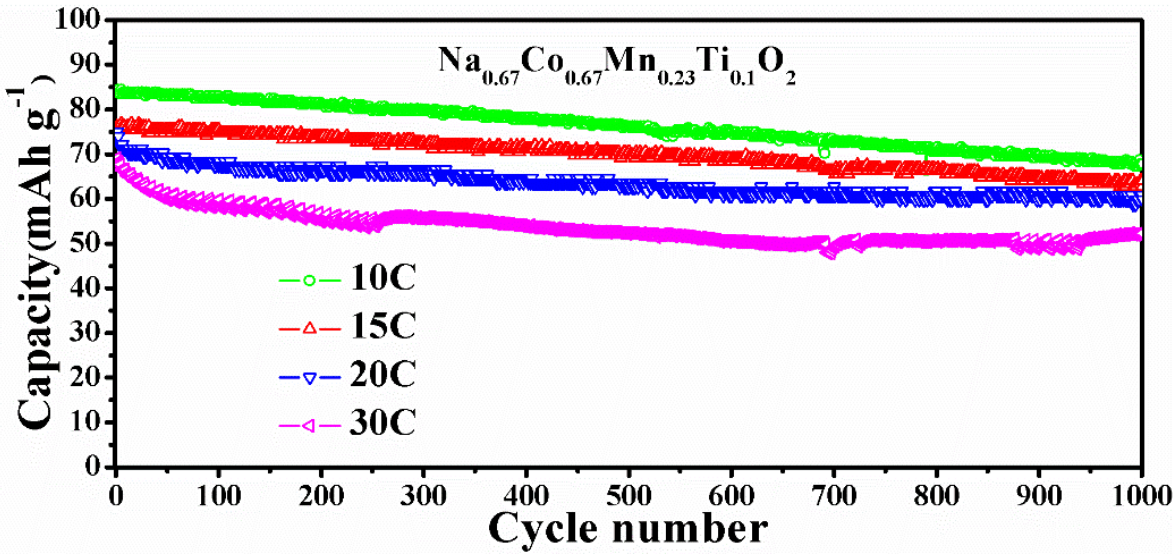

Figure 5. Cycling performance at 10C, 15C, 20C, and 30C for 1000 cycles of $Na_{0.67}Co_{0.67}Mn_{0.23}Ti_{0.1}O_2$.

Table 2. Summary of the sodium storage performance of cathode materials

Materials	Synthesis method	Cut-off voltage	Initial discharge capacity(mAh g^{-1})	Capacity retention	Ref.
$Na_\chi Co_{0.7}Mn_{0.3}O_2$ ($\chi \approx 1$)	Co-precipitation and solid state reaction	2-4.1V	95 @1C	84% after 225 cycles at 1C	9
$Na_{0.66}Co_{0.5}Mn_{0.5}O_2$	Sol-gel	1.5-4.3V	126.6 @5C	77% after 100 cycles at 5C	22
$NaCo_{1/2}Fe_{1/2}O_2$	Solid state reaction	2.5-4.0	160@ C /20	90% after 50 cycles at C /20	23
$NaNi_{1/3}Co_{1/3}Fe_{1/3}O_2$	Solid state reaction	2-4.2V	165@ C /20	94% after 10 cycles at C /20	26
$Na_{2/3}Co_{2/3}Mn_{2/9}Ni_{1/9}O_2$	Sol-gel	2-4.2V	110@ C /20	89% after 90 cycles at C /20	27
$Na_{2/3}Ni_{1/3}Mn_{1/2}Ti_{1/6}O_2$	Solid state reaction	2.5-4.2V	110@ C /20	94% after 10 cycles at C /20	29
$NaNi_{0.5}Mn_{0.2}Ti_{0.3}O_2$	Solid state reaction	2-4.0V	135 @0.05C	85% after 200 cycles at 1C	30
$Na_{0.67}Co_{0.67}Mn_{0.23}Ti_{0.1}O_2$	Solid state reaction	2-4.2V	91.2 @1C	81.02% after 1000 cycles at 20C	this paper

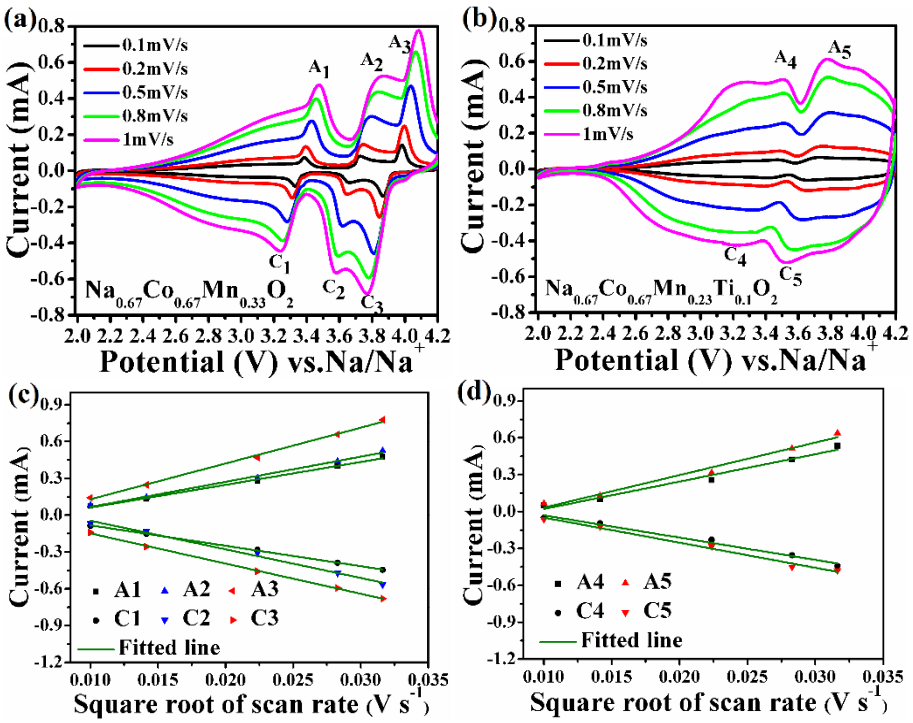

Figure 6. CV curves of (a) $Na_{0.67}Co_{0.67}Mn_{0.33}O_2$ and (b) $Na_{0.67}Co_{0.67}Mn_{0.23}Ti_{0.1}O_2$ at various scan rates from 0.1 to 1mV/s, (c) and (d) Variation of the peak current vs. square root of the scan rates ($v^{1/2}$).

The plots of the peak currents versus $v^{1/2}$ of the two samples display well linear relationship (see Fig. 6c and d), suggesting that the intercalation/deintercalation of Na^+ is a diffusion-controlled process [49]. It is very important to explore the diffusion capability of Na-ions. The Randles-Sevcik was used to calculate the Na-ion diffusion coefficients D. The formula can be written as:

$Ip = 2.69*10^5 An^{3/2} CoD^{1/2} v^{1/2}$

where Ip is the peak current (A), A is the the effective contact area between the electrode and electrolyte (cm^2), n is the number of electrons in the reaction, Co is the concentration of Na^+, D is the

diffusion coefficient of Na^+, v is the CV scanning rate. The peak A1 and A4 were chosen to calculate D, which corresponding to the sample $Na_{0.67}Co_{0.67}Mn_{0.33}O_2$ and $Na_{0.67}Co_{0.67}Mn_{0.23}Ti_{0.1}O_2$. The derived results D_{Na+} of $3.6*10^{-12}$ cm^2/s ($Na_{0.67}Co_{0.67}Mn_{0.23}Ti_{0.1}O_2$) is relatively higher than that of $2.5*10^{-12}$ cm^2/s ($Na_{0.67}Co_{0.67}Mn_{0.33}O_2$), which indicate a better performance of the cathode.

EIS spectra of $Na_{0.67}Co_{0.67}Mn_{0.33}O_2$ and $Na_{0.67}Co_{0.67}Mn_{0.23}Ti_{0.1}O_2$ was performed in the frequency range between 100 KHz and 0.01 Hz with 5 mV amplitude of AC signal, as shown in Fig. 7. Both the curves are composed of two anomalous semicircles in the high and intermediated frequency and a slope in the lower frequency. The intercept at the real axis (Z') in the high region is contributed mainly by the resistance of the electrolyte and cathode (Rs). The semicircle in the intermediated frequency is related to the process of sodiation/desodiation, which can be presented by the charge transfer resistance (R_{ct}). Apparently, the radius in the intermediated frequency of $Na_{0.67}Co_{0.67}Mn_{0.23}Ti_{0.1}O_2$ is smaller than that of $Na_{0.67}Co_{0.67}Mn_{0.33}O_2$, indicating the easier Na^+ transfer during the sodium insertion and extraction, which probably result in higher cyclability and high-rate performance. Furthermore, the semicircle of $Na_{0.67}Co_{0.67}Mn_{0.23}Ti_{0.1}O_2$ in the intermediated frequency is more close to the real axis suggest that the conductivity increases. The sloping line in the low frequency that represents the sodium-ion diffusion resistance in the electrode material, named the Warburg impedance.

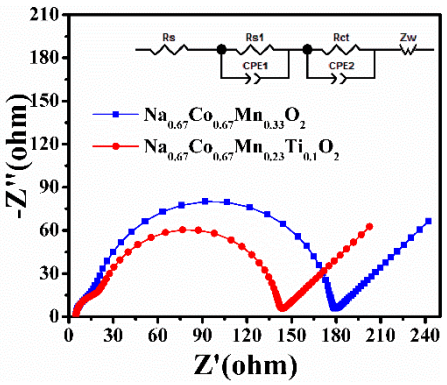

Figure 7. EIS spectra of $Na_{0.67}Co_{0.67}Mn_{0.33}O_2$ and $Na_{0.67}Co_{0.67}Mn_{0.23}Ti_{0.1}O_2$.

4. CONCLUSIONS

In summary, a series of novel P2-type $Na_{0.67}Co_{0.67}Mn_{0.33-\chi}Ti_{\chi}O_2$ ($0\leq \chi \leq 0.2$) cathode materials with eminent performance were successfully synthesized by solid-state approach. The charge and discharge profile of $Na_{0.67}Co_{0.67}Mn_{0.33-\chi}Ti_{\chi}O_2$ (χ=0.1, 0.15, and 0.2) electrodes have been smoothed due to the suppression of multiphase transformation through partial Ti-doping. Consequently, the optimized $Na_{0.67}Co_{0.67}Mn_{0.23}Ti_{0.1}O_2$ cathode delivers a higher reversible capacity of 91.2 mAh g^{-1} at 1C, as well as superior rate performance with ultra long cycle life (retaining 81.02% of its initial capacity after 1000 cycles at 20C). The outstanding electrochemical performance indicates that $Na_{0.67}Co_{0.67}Mn_{0.23}Ti_{0.1}O_2$ can be used as cathode materials for SIBs with superior rate capability and long cycling stability.

ACKNOWLEDGEMENTS
This work was supported by the Science and Technology Inno-vation Team of Sichuan Province (No. 2015TD0003)

References

1. J.B. Goodenough, Y. Kim, *Chem. Mater.*, 22 (2010) 587.
2. H. Yu, H. Zhou, *J Phys Chem Lett*, 4 (2013) 1268.
3. C.X. Zu, H. Li, *Energy Environ. Sci.*, 4 (2011) 2614.
4. Z. Yang, J. Zhang, M.C. Kintner Meyer, X. Lu, D. Choi, J.P. Lemmon, J. Liu, *Chem Rev*, 111 (2011) 3577.
5. R.J. Clément, P.G. Bruce, C.P. Grey, *J. Electrochem. Soc.*, 162 (2015) A2589.
6. S. Komaba, W. Murata, T. Ishikawa, N. Yabuuchi, T. Ozeki, T. Nakayama, A. Ogata, K. Gotoh, K. Fujiwara, *Adv. Funct. Mater.*, 21 (2011) 3859.
7. S.M. Oh, S.T. Myung, C.S. Yoon, J. Lu, J. Hassoun, B. Scrosati, K. Amine, Y.K. Sun, *Nano Lett.*, 14 (2014) 1620.
8. N. Recham, J.N. Chotard, L. Dupont, K. Djellab, M. Armand, J.M. Tarascon, *J. Electrochem. Soc.*, 156 (2009) A993.
9. Y. Shen, S. Birgisson, B.B. Iversen, *J. Mater. Chem. A*, 4 (2016) 12281.
10. S. Difi, I. Saadoune, M.T. Sougrati, R. Hakkou, K. Edstrom, P.E. Lippens, *J. Phys. Chem. C*, 119 (2015) 25220.
11. K. Saravanan, C.W. Mason, A. Rudola, K.H. Wong, P. Balaya, *Adv. Energy Mater.*, 3 (2013) 444.
12. J. Yan, X. Liu, B. Li, *Electrochem. Commun.*, 56 (2015) 46.
13. Z. Wang, W. He, X. Zhang, Y. Yue, G. Yang, X. Yi, Y. Wang, J. Wang, *ChemElectroChem*, 4 (2017) 671.
14. M.H. Han, E. Gonzalo, G. Singh, T. Rojo, *Energy Environ. Sci.*, 8 (2015) 81.
15. C. Delmas, C. Fouassier, P. Hagenmuller, *Physica B & C*, 99 (1980) 81.
16. S.W. Kim, D.H. Seo, X. Ma, G. Ceder, K. Kang, *Adv. Energy Mater.*, 2 (2012) 710.
17. Q. Huang, M.L. Foo, R.A. Pascal, J.W. Lynn, B.H. Toby, T. He, H.W. Zandbergen, R.J. Cava, *Physical Review B*, 70 (2004)184110.
18. R. Berthelot, D. Carlier, C. Delmas, *Nat Mater*, 10 (2011) 74.
19. J.J. Ding, Y.N. Zhou, Q. Sun, X.Q. Yu, X.Q. Yang, Z.W. Fu, *Electrochim. Acta*, 87 (2013) 388.
20. M. Medarde, M. Mena, J.L. Gavilano, E. Pomjakushina, J. Sugiyama, K. Kamazawa, V.Y. Pomjakushin, D. Sheptyakov, B. Batlogg, H.R. Ott, M. Mansson, F. Juranyi, *Phys. Rev. Lett.*, 110 (2013) 266401.
21. D. Carlier, J.H. Cheng, R. Berthelot, M. Guignard, M. Yoncheva, R. Stoyanova, B.J. Hwang, C. Delmas, *Dalton Trans.*, 40 (2011) 9306.
22. X. Chen, X. Zhou, M. Hu, J. Liang, D. Wu, J. Wei, Z. Zhou, *J. Mater. Chem. A*, 3 (2015) 20708.
23. H. Yoshida, N. Yabuuchi, S. Komaba, *Electrochem. Commun.*, 34 (2013) 60.
24. D. Baster, W. Zając, Ł. Kondracki, F. Hartman, J. Molenda, Solid State Ionics. 288(2016)213.
25. M. Sathiya, K. Hemalatha, K. Ramesha, J.M. Tarascon, A.S. Prakash, *Chem. Mater.*, 24 (2012) 1846.
26. P. Vassilaras, A.J. Toumar, G. Ceder, *Electrochem. Commun.*, 38 (2014) 79.
27. S. Doubaji, M. Valvo, I. Saadoune, M. Dahbi, K. Edström, *J.Power Sources*, 266 (2014) 275.
28. V.S. Rangasamy, S. Thayumanasundaram, J.-P. Locquet, J.W. Seo, *Ionics*, 23 (2016) 645.
29. H. Yoshida, N. Yabuuchi, K. Kubota, I. Ikeuchi, A. Garsuch, M. Schulz-Dobrick, S. Komaba, *Chem Commun (Camb)*, 50 (2014) 3677.
30. P.F. Wang, H.R. Yao, X.Y. Liu, J.N. Zhang, L. Gu, X.Q. Yu, Y.X. Yin, Y.G. Guo, *Adv. Mater.*, (2017) 1700210.

31. J. Billaud, G. Singh, A.R. Armstrong, E. Gonzalo, V. Roddatis, M. Armand, T. Rojo, P.G. Bruce, *Energy Environ. Sci.*, 7 (2014) 1387.
32. P.F. Wang, Y. You, Y.X. Yin, Y.S. Wang, L.J. Wan, L. Gu, Y.G. Guo, *Angew. Chem. Int. Ed. Engl.*, 55 (2016) 7445.
33. Paulsen JM, Dahn JR, *Solid State Ionics*, 126 (1999)3.
34. Tournadre F, Croguennec L, Saadoune I, Weill F, Shao-Horn Y, Willmann P. and Delmas C, *Chem. Mater.*, 16(2004)1411.
35. M.H. Han, E. Gonzalo, N. Sharma, J.M. López del Amo, M. Armand, M. Avdeev, J.J. Saiz Garitaonandia, T. Rojo, *Chem. Mater.*, 28 (2016) 106.
36. X. Sun, Y. Jin, C.Y. Zhang, J.W. Wen, Y. Shao, Y. Zang, C.H. Chen, *J. Mater. Chem. A*, 2 (2014) 17268.
37. J.L. Yue, W.W. Yin, M.H. Cao, S. Zulipiya, Y.N. Zhou, Z.W. Fu, *Chem Commun (Camb)*, 51 (2015) 15712.
38. J.L. Yue, Y.N. Zhou, X. Yu, S.M. Bak, X.Q. Yang, Z.W. Fu, *J. Mater. Chem. A*, 3 (2015) 23261.
39. P.F. Wang, Y. You, Y.X. Yin, Y.G. Guo, *J. Mater. Chem. A*, 4 (2016) 17660.
40. S. Liu, X. Jiang, J. Zhang, J. Yang, Y. Qian, *RSC Adv.*, 6 (2016) 55327.
41. D. Yuan, W. He, F. Pei, F. Wu, Y. Wu, J. Qian, Y. Cao, X. Ai, H. Yang, *J. Mater. Chem. A*, 1 (2013) 3895.
42. N.V. Nghia, P.W. Ou, I.M. Hung, *Ceram. Int.*, 41 (2015) 10199.
43. X. Sun, X.Y. Ji, H.Y. Xu, C.Y. Zhang, Y. Shao, Y. Zang, C.-H. Chen, *Electrochim. Acta*, 208 (2016) 142.
44. N. Yabuuchi, M. Kajiyama, J. Iwatate, H. Nishikawa, S. Hitomi, R. Okuyama, R. Usui, Y. Yamada, S. Komaba, *Nat Mater*, 11 (2012) 512.
45. F.R. Beck, Y.Q. Cheng, Z. Bi, M. Feygenson, C.A. Bridges, Z. Moorhead-Rosenberg, A. Manthiram, J.B. Goodenough, M.P. Paranthaman, A. Manivannan, *J. Electrochem. Soc.*, 161 (2014) A961.
46. J.H. Park, K. Park, R.H. Kim, D.J. Yun, S.Y. Park, D. Han, S.S. Lee, J.H. Park, *J. Mater. Chem. A*, 3 (2015) 10730.
47. X. Zhou, R.K. Guduru, P. Mohanty, *J. Mater. Chem. A*, 1 (2013) 2757.
48. J. Liu, J. Wang, Z. Ku, H. Wang, S. Chen, L. Zhang, J. Lin, Z.X. Shen, *ACS Nano*, 10 (2016) 1007.
49. L.J. Xi, H.E. Wang, Z.G. Lu, S.L. Yang, R.G. Ma, J.Q. Deng, C.Y. Chung, *J.Power Sources*, 198 (2012) 251.

© 2018 The Authors. Published by ESG (www.electrochemsci.org). This article is an open access article distributed under the terms and conditions of the Creative Commons Attribution license (http://creativecommons.org/licenses/by/4.0/).